1   # Dual control of meiotic crossover patterning

2   Stéphanie Durand[1]*, Qichao Lian[1]*, Juli Jing[1]*, Marcel Ernst[2], Mathilde Grelon[3], David

3   Zwicker[2] and Raphael Mercier[1#]

4   [1] Department of Chromosome Biology, Max Planck Institute for Plant Breeding Research,

5   Carl-von-Linné-Weg 10, 50829 Cologne, Germany

6   [2] Max Planck Institute for Dynamics and Self-Organization, Am Faßberg 17, 37077 Göttingen,

7   Germany

8   [3] Université Paris-Saclay, INRAE, AgroParisTech, Institut Jean-Pierre Bourgin (IJPB), 78000,

9   Versailles, France

10

11   * Contributed equally to this work

12   # corresponding author. mercier@mpipz.mpg.de

13

14   Most meiotic crossovers (COs), called class I crossovers, are produced by a conserved pathway

15   catalyzed by the ZMM proteins; COs are limited in number, typically to 1–3 per chromosome,

16   and are prevented from occurring close to one other by crossover interference[1-3]. In many

17   species, CO number is subject to dimorphism between males and females, and a lower CO

18   number is associated with shorter chromosome axes and stronger interference[4]. How the

19   patterning of COs is imposed, however, remains poorly understood. Here, we show that

20   overexpression of the ZMM protein HEI10 increases COs and reduces crossover interference

21   but maintains sexual dimorphism; shorter axes length in female meiosis is still associated with

22   fewer COs and stronger interference than in male meiocytes. Disrupting the synaptonemal

23   complex (SC) by mutating *ZYP1* also leads to an increase in class I COs but, in contrast,

24   abolishes interference and disrupts the link between chromosome axis length and COs, with

25   female and male meiocytes having the same CO frequency despite different axis lengths.

26   Combining HEI10 overexpression and *zyp1* mutation leads to a massive increase in class I COs

27   and absence of interference, while axes lengths are still unaffected. These observations support,

28   and can be effectively predicted by, a recently proposed coarsening model[5,6] in which HEI10

29   diffusion is funneled by the central element of the SC before coarsening into large, well-spaced

30   CO-promoting droplets. Given the conservation of the components, this model may account

31   for CO patterning in many eukaryotes.

Introduction

33   A hallmark of sexual reproduction is the shuffling of homologous chromosomes by

34   meiotic crossovers (COs). COs are produced by the repair of DNA double-strand breaks

35   through two biochemical pathways: Class I COs are produced by a meiotic-specific pathway

36   catalyzed by the ZMM proteins (*Saccharomyces cerevisiae* Zip1-4, Msh4-5, and Mer3) and

37   represent most COs; Class II COs originate from a minor pathway that uses structure-specific

38   DNA nucleases also implicated in DNA repair in somatic cells. Despite a vast excess of initial

39   double-strand breaks, the number of resulting COs is limited, typically to one to three per

40   chromosome pair. Class I COs are subject to additional tight constraints: At least one class I

41   CO occurs per chromosome pair at each meiosis, the so-called obligate CO that ensures

42   balanced chromosome distribution. Class I COs are also prevented from occurring next to each

43   other on the same chromosome, a phenomenon called crossover interference. How this

44   interference is achieved mechanistically has been debated for over a century[1,3,7-9].

45   One specific unresolved question is the role of the synaptonemal complex (SC) in crossover

46   interference. The SC is a zipper-like tripartite structure composed of two lateral chromosome

47   axes, along which arrays of chromatin loops of each of the two homologous chromosomes are

48   anchored, and a central part consisting of transverse filaments that connect the axes all along

49   their length at meiotic prophase. Assessing the role of the SC in interference is difficult,

50   because in many organisms the transverse filament protein is essential for the formation of

51   class I COs[2]. One notable exception is *Arabidopsis thaliana*, where the transverse filament

52   protein is not required for class I CO formation, providing a unique opportunity to analyze the

53   role of the SC in CO patterning. In the *zyp1* mutant, class I COs form at a higher frequency

54   than wild type and completely lack interference, demonstrating that the central element of the

55   SC is, directly or indirectly, essential for imposing CO interference in Arabidopsis[10,11].

56   Reduced expression of the transverse element in *C. elegans* and specific mutations of the SC

57   component that uncouple SC and CO formation in budding yeast lead to a reduction of

58   interference, supporting a conserved role of the SC in imposing interference[12-15]. Interestingly

59   in some species, such as humans or Arabidopsis, CO number differs in males and females. This

60   heterochiasmy correlates with axis/SC length, with the number of COs proportional to axis

61   length[4,16,17]. CO interference appears to propagate at a similar axis/SC distance (μm) in both

62   sexes, which means that interference acts over greater genomic ranges (DNA) in the sex with

63   a shorter axis/SC[17,18], an observation which shows that the relevant space for the mechanism

64   of interference is the axis/SC length.

65   A model was recently elaborated to account for class I CO patterning and interference,

66   based on diffusion of the ZMM protein HEI10 (ZHP-3/4 in *C.elegans*) within the SC and a

67   coarsening process leading to well-spaced CO-promoting HEI10 droplets[5,6]. HEI10, which

68   encodes an E3 ubiquitin ligase, initially forms multiple small foci along the SC and is

69   progressively consolidated into a small number of large condensates that co-localize with CO

70   sites in diverse species[19-22]. Further, as predicted by the model, CO numbers depend on HEI10

71   dosage in Arabidopsis[6,23]. Interference is abolished in the absence of the transverse element of

72   the synaptonemal complex ZYP1[10,11], which is compatible with the idea that diffusion of

73   HEI10 along the central part of the SC underlies crossover patterning and interference.

74   Here, we explored the mechanisms of CO patterning in Arabidopsis by analyzing the

75   combinatory effects of axis/SC length (male vs. female), modification of HEI10 dosage, and

76   disruption of the SC on COs. We notably show that overexpressing HEI10 in *zyp1* completely

77   deregulates class I COs, with a massive increase of their number in both females and males.

78   Our results support the model in which HEI10 coarsening by diffusion along the central

79   element of the SC mediates CO patterning and imposes CO interference.

80   **Results and discussion:**

81   To decipher CO control, we studied the number and distribution of COs in both female

82   and male meiosis when overexpressing HEI10 (well-characterized C2 line[23]), in the absence of

83   the synaptonemal complex (*zyp1*), and in combination. We measured the number of class I

84   COs in meiocytes by counting the number of MLH1-HEI10 co-foci at diplotene. In the pure

85   line Col we analyzed six genotypes: wild type and *zyp1-1* combined with three dosages or

86   HEI10 (wild type, heterozygous or homozygous for the HEI10[oe] C2 transgene). In the Col/L*er*

87   F1 hybrid, we analyzed four genotypes: wild type and *zyp1-1/zyp1-6* combined with two

88   dosages of HEI10 (wild type and heterozygous for the C2 HEI10 transgene) (Figure 1A-B).

89   The four hybrid genotypes were also used to characterize the crossover number and distribution

90   by sequencing populations derived from female and male crosses to Col (Figure 1C–F, Figure

91   2, Figure S1–4).

92   **Overexpression of HEI10 increases COs but maintains heterochiasmy**

93   In wild types, the number of MLH1 foci is higher in males than females in both the

94   inbreds and the hybrids (ratio male/female=1.8 and 1.6, respectively. Figure 1A–B). Whole-

95   genome sequencing of male- and female-derived hybrid progenies showed that CO numbers

96   detected genetically are higher in male meiosis than in female meiosis (Figure 1D, ratio=1.6,

97    $p<0.001$), confirming heterochiasmy. The number of MLH1 foci at male meiosis is higher in

98   wild-type Col than in Col/L*er*. Analysis of quantitative trait loci (QTL) in a Col/L*er* population

99   previously revealed that the Col *HEI10* allele is associated with higher recombination levels,

100   suggesting that at least a part of this difference in MLH1 counts can be attributed to a difference

101   in HEI10 activity[23]. In wild-type female, the MLH1 foci numbers are not significantly different

102   between Col and Col/L*er* and close to the minimum of one per chromosome (7.2 and 6.8 foci

103   for five chromosomes). In the presence of a transgene ectopically overexpressing HEI10

104   (HEI10[oe] C2 line [23], homozygous), the number of MLH1 is increased ~two-fold in both sexes,

105   in both Col and Col/L*er*. Heterozygosity for the HEI10[oe] transgene also increases MLH1 foci

106   number, but slightly less than homozygosity, confirming the effect of HEI10 dosage on

107   recombination[6,23] and suggesting that the level of HEI10 in the C2 line is close to saturation.

108   Importantly, increases provoked by HEI10 dosage modulation are similar in males and females,

109   leading to more MLH1 in males than females ($p=0.0001$) (Figure 1B). This was confirmed

110   with progeny sequencing in hybrids, which revealed a 2.1-fold increase of COs in HEI10[oe]

111   female and male, compared with wild type ($p < 2.2e-16$, Figure 1D-F). The ratio of male vs.

112   female COs is maintained at 1.6 in HEI10[oe] ($p < 2.2e-16$). In summary, overexpressing HEI10

113   provokes a doubling of class I COs in both female and male, maintaining heterochiasmy.

114   ***ZYP1* mutation increases COs and abolishes heterochiasmy**

115   Mutating the transverse element of the SC ZYP1 also increases MLH1 foci number (Figure

116   1B). In Col *zyp1,* compared to wild type, the numbers increased 1.4-fold in males, consistent

117   with previous findings[10,11], and 2.3-fold in females. In the Col/L*er* hybrid, the numbers

118   increased by 1.2-fold in male and 1.8-fold in females. In contrast to HEI10[oe], MLH1 foci

119   number is no longer significantly different in males versus females ($p>0.6$). This is consistent

120   with genetic crossovers detected by sequencing of hybrid progenies with equal numbers

121   observed in female and male gametes and fold increases of 2.3 in females and 1.5 in males

122   compared to wild type (Figure 1D)[11]. The *zyp1* mutation thus leads to an increase in class I

123   COs, which disproportionately affects female meiosis and abolishes heterochiasmy.

124   **Combining HEI10 overexpression and *zyp1* massively increases class I COs.**

125   HEI10^{oe} and *zyp1* increase CO number, but in different ways; while the former maintains

126   heterochiasmy, the latter does not. We thus combined *zyp1* mutation and HEI10^{oe} and analyzed

127   the effects on MLH1 foci numbers (Figure 1A–B). In Col, the number of foci observed in *zyp1*

128   mutants homozygous for the HEI10^{oe} transgene was significantly higher than ever previously

129   reported, reaching 47.8 and 45.0 in females and males, respectively. The female and male

130   MLH1 counts are not significantly different from each other and represent marked 6.7-fold and

131   3.5-fold increases compared to their respective wild types. In Col *zyp1* males heterozygous for

132   HEI10^{oe}, the MLH1 foci count was slightly but significantly lower (41.1, p=0.015) than the

133   homozygous, showing that there is a dynamic range of HEI10 dosage effects on COs. In the

134   hybrid *zyp1* HEI10^{oe}, the observed number of MLH1 in females and males was 29.8 and 30.0,

135   not significantly different from each other (p=0.8) but representing a 4.4- and 2.9-fold increase

136   compared to their wild-type controls. This suggests that class I COs are massively increased in

137   *zyp1* mutants overexpressing HEI10. Indeed, progeny sequencing showed that the number of

138   genetic COs in male *zyp1* HEI10^{oe} was dramatically increased compared to wild type, reaching

139   14.7 CO per gamete (3.1-fold, Mann-Whitney test, p < 2.2e-16, Figure 1D-F), fitting well with

140   the 30 MLH1 foci counted in male meiocytes (Figure 1B). In females, COs were also vastly

141   increased, but intriguingly, to even higher levels than predicted by the number of MLH1 foci

142   (30/2=15), reaching a striking 19.6 COs per female gamete (6.4-fold/wild type, p < 2.2e-16,

143   Figure 1D–F). Together, this shows that combining *zyp1* mutation and HEI10 overexpression

144   cumulatively and massively increases the numbers of class I COs. It also suggests that class II

145   COs may also be increased in female *zyp1* HEI10^{oe}. Such an increase in class I COs is

146   unprecedented, and suggests that the central element of the SC and HEI10 levels are two main

147   regulators limiting class I COs.

148   Looking along chromosomes, *zyp1* and HEI10^{oe} individually or in combination elicit a massive

149   increase in COs along the arms while the peri-centromeres and the Col/L*er* large inversion[24,25]

150   remained recalcitrant to recombination (Figure 2, Figure S3). At the fine scale, the majority of

151   COs were located in genic regions in both wild type and mutants (Figure S4). This suggests

152   that despite a large increase in CO number, the local preference for CO placement is conserved,

153   presumably because the distribution of double-strand breaks is maintained. For all eight hybrid

154   populations, the average observed number of COs is positively correlated with the physical

155   size of chromosomes (Pearson's correlation coefficients >0.8, Figure 1E). We looked for co-

156   variation of CO frequency between chromosomes within the same meiocyte/gamete, as

157   observed in various species[26]. No significant correlation was seen in any of the populations,

158   with maximum correlation coefficients of ~0.2 observed in female *zyp1* HEI10[oe] (Figure S2),

159   suggesting that this co-variation does not exist in Arabidopsis or is too small to be detected in

160   our essay.

161   **CO interference is reduced by HEI10 overexpression and abolished in *zyp1***

162   To measure the impact of *zyp1* and HEI10[oe] on CO interference, we first analyzed the

163   distribution of distances between two genetically detected COs for chromosomes with exactly

164   two COs in female and male gametes (Figure 2). In wild-type females and males, the

165   distribution was significantly shifted to large inter-CO distances ($p<10^{-6}$) compared with the

166   expected distribution if the COs were randomly spaced, showing the presence of CO

167   interference (Figure 2C). In HEI10[oe] females and males, the distribution was also shifted to

168   longer distances, showing the presence of CO interference in both sexes ($p<10^{-4}$, Figure 2D).

169   However, the shift was less marked than in the wild type, suggesting a reduction of interference

170   in HEI10[oe]. In *zyp1* and *zyp1* HEI10[oe], the observed distributions of inter-CO distances were

171   not different from what would be expected in the case of random spacing ($p>0.2$, Figure 2E–

172   F), suggesting an abolition of CO interference in both females and males. Furthermore, we

173   performed a coefficient of coincidence (CoC curve) analysis for an alternative, likely more

174   accurate, measurement of CO interference (Figure 2G-J)[9]. In wild type, the two CoC curves

175   are below 1 at distances <~15 Mb in both females and males, confirming the presence of

176   substantial CO interference (Figure 2G). The female curve stays close to 0 for longer distances,

177   showing that CO interference propagates to longer Mb distances in females, consistent with

178   previous analyses[11,16,18]. In HEI10[oe], the curves also deviate from 1 at short distances (<~7Mb),

179   showing the presence of interference, although at a reduced level compared to wild type (Figure

180   2H). As in wild type, interference in HEI10[oe] is stronger in female than in male meiosis. In

181   contrast, the CoC curves are flat at values close to 1 for both females and males in *zyp1* (Figure

182   2I), confirming that CO interference is abolished in the absence of ZYP1[10,11]. In *zyp1* HEI10[oe],

183   the curves are also flat at ~1, showing that the numerous class I COs produced in this context

184   do not interfere with each other (Figure 2J). Thus, HEI10[oe] reduces, while *zyp1* abolishes CO

185   interference.

186   **High CO rates in *zyp1* and HEI10[oe] are not associated with meiotic defects**

187   The limited level of COs per chromosome observed in most eukaryotes could suggest that a

188   high level of COs has a detrimental effect. We explored if a massive elevation of class I COs

189   is associated with meiotic chromosome segregation and fertility defects. The number of seeds

190   per fruit is reduced in *zyp1-1* compared to wild type (-8%, t-test p<0.001), consistent with

191   previous results and the reported loss of the obligate CO in *zyp1* mutants[10,11] (Figure 3I).

192   Analyses based on sequence coverage detected a few aneuploids among *zyp1* gametes (2/497,

193   Figure 3J and S6–7) that were not detected in hybrid wild types (0/427 in this study, and 0/760

194   in an independent wild-type dataset[27]). The HEI10[oe] C2 line also showed a slight reduction of

195   fertility (-12%, p=0.005, Figure 3I) and low frequency of aneuploid gametes (2/285). In *zyp1*

196   HEI10[oe], seed number was reduced (-7%, p=0.025), and a small number of aneuploids were

197   detected in hybrids (7/272), suggesting a slight meiotic defect also in this background. All the

198   11 identified trisomy cases concerned chromosome 4, the shortest Arabidopsis chromosome.

199   The centromeric region of chromosome 4 of the aneuploid gamete is systematically

200   heterozygous Col/L*er*, which is diagnostic for missegregation at meiosis I (failure to separate

201   homologous chromosomes). For the vast majority (9/11), no CO was detected on the aneuploid

202   chromosome, which is compatible with an absence of COs in the bivalent. This suggests that

203   these nine events resulted from the loss of the obligate crossover and consequent random

204   missegregation of homologs. Two aneuploids, both from *zyp1* HEI10[oe], had two COs on the

205   trisomic chromosome. In both cases, the two COs are relatively close to each other (~2 and 4

206   Mb), which may lead to an unstable connection between the homologs as spindle tension would

207   be counteracted by only a short stretch of cohesion. The aneuploidies appear thus to be

208   associated with the absence of COs or specific configurations of a pair of COs. Meiotic

209   chromosome spreads in *zyp1* HEI10[oe] showed that most metaphase I cells had a wild-type

210   configuration with five bivalents aligned on the metaphase plate (44/45 in Col; 23/30 in

211   Col/L*er*; Figure 3C). However, one univalent was observed in a minority of cells (1/45 and

212   7/30, Figure 3C). Consistently, at metaphase II almost all cells had five chromosomes aligned

213   on the two plates (25/25 and 6/7; Figure 3D), and one had a 6:4 configuration indicating

214   unbalanced segregation at meiosis I (Figure E, F), likely due to the absence of the obligate CO.

215   Altogether, this shows that a slight meiotic chromosome segregation defect is present in

216   HEI10[oe] *zyp1*. However, the rare missegregations appear to be due to an incomplete CO

217   assurance and are not associated with the extreme CO numbers observed in the mutants (up to

218   15 COs in a single chromatid, Table S4). This suggests that high CO number does not impair

219   chromosome segregation and raises the question of the evolutionary forces that limit CO to

220   typically less than three per chromosome per meiosis in most eukaryotes[1,28]. While failure to

221   insure at least one CO per chromosome pair is associated with meiotic failure in most

222   eukaryotes, the reasons that prevent high CO number are unclear. The absence of an immediate

223   cost of massively elevated CO numbers in HEI10[oe] *zyp1* suggests that low CO numbers are not

224   selected for by evolution because of mechanical constraints during meiosis. Rather, this

225   observation suggests that the medium-to-long term genetic effects of COs are subject to indirect

226   selection[1]. This supports the suggestion that a relatively low recombination rate, not much

227   higher than one per chromosome, is optimal for adaptation.

228   **Female and male SC lengths differ and are affected by neither HEI10[oe] nor *zyp1***

229   SC length has been shown to correlate with the frequency of class I COs[4,16,17]. We wondered if

230   the class I CO increase provoked by *zyp1* and HEI10[oe] is associated with variation in SC length.

231   We traced chromosome axis (REC8) in female and male meiocytes with preserved 3D

232   organization and measured the length of each chromosome (Figure 4, Table S5). In wild type,

233   we found that the SC is 1.6-fold longer in males than females, consistent with previous reports[16]

234   (Figure 4M). The longer total SC length in wild-type males is proportional to the higher MLH1

235   foci and CO numbers compared to females (Figure 1B, 1D, 4Q), suggesting that SC length

236   determines CO number and thus drives heterochiasmy. Strikingly SC/axis absolute and relative

237   length is conserved in both sexes in HEI10[oe], *zyp1,* and *zyp1* HEI10[oe] mutants, thus maintaining

238   the male-female dimorphism (Figure 4M). In HEI10[oe], the MLH1 foci and CO numbers are

239   increased proportionally in males and females, maintaining heterochiasmy (Figure 1B, 4O–Q).

240   This suggests that the effect of HEI10 dosage on COs is constrained by the length of the SC.

241   In clear contrast to HEI10[oe], the link between axis length and CO number is disrupted in *zyp1*,

242   with MLH1 foci and COs equal in males and females despite a large difference in axis length

243   (4O–Q). The observation that the length of pairs of axes in *zyp1* matches the length of the

244   assembled SC in the wild type suggests that the length of the two axes directly determines SC

245   length. In the double mutant *zyp1* HEI10[oe], MLH1 foci are massively increased and reach equal

246   numbers in males and females despite different axis lengths that are unmodified compared to

247 wild type (Figure 4P). This suggests that HEI10 dosage has a comparable effect in males and

248 females in the absence of the SC.

249 Altogether, this suggests that two major factors conjointly regulate CO number: (i) Our results

250 show that the central element of the SC ZYP1 imposes interference and limits COs. The length

251 of the axis/SC is correlated with the number of COs in various contexts[4], and notably when

252 comparing sexes. Crucially, this correlation is lost in the absence of ZYP1, where the difference

253 in axis length is no longer associated with a difference in CO number, suggesting that COs are

254 regulated by the length of the tripartite SC and thus indirectly by the axis. The upstream

255 mechanisms that determine the differences in SC lengths in males and females in many

256 organisms remain to be determined. (ii) HEI10 dosage positively regulated CO formation. The

257 effect of HEI10 dosage appears to be constrained by the length of the SC. HEI10 initially loads

258 as multiple foci along the SC before consolidating into a small number of large foci at CO

259 sites[19]. This supports a model in which HEI10 loading on the SC depends conjointly on HEI10

260 expression levels and SC length and that this loading eventually determines CO number.

261 **The HEI10 coarsening model**

262 The results we present here and previous observations can be interpreted in the context of an

263 emerging model for crossover patterning via droplet coarsening through the diffusion of HEI10

264 along the SC[5,6]. In this model (Figure 5), HEI10 initially forms multiple droplets along the SC,

265 and HEI10 molecules diffuse along the SC from droplets to droplets. If larger droplets tend to

266 retain more HEI10 molecules than smaller droplets, a coarsening process is initiated, and large

267 droplets grow at the expense of nearby smaller droplets, leading to the formation of well-spaced

268 large droplets. These large droplets are proposed to create a specific context that promotes class

269 I CO formation (e.g., by attracting the MLH1/MLH3 complex) and protects recombination

270 intermediates from anti-CO factors (i.e., FANCM and RECQ4[29,30]). It is unclear if initial

271 droplets colocalize with recombination intermediates or if recombination intermediates favor

272 the coarsening process locally, but both hypotheses envisage final droplets to embed such an

273 intermediate. This model predicts the obligate crossover, a limited number of COs, and

274 interference[6]. If the coarsening process can proceed without restrictions, it would ultimately

275 lead to the formation of a single droplet/CO per bivalent, as observed in *C. elegans*[5]. However,

276 in most species, including Arabidopsis, 2–3 interfering class I COs are typically observed per

277 bivalent. At least three hypotheses can account for this observation: one proposes an upper

278 limit in the size of a droplet, above which it stops growing, allowing other droplets to be

279   maintained. The second supposes that the coarsening is stopped when a checkpoint is satisfied
280   (e.g., when a least one large droplet/one CO is formed per chromosome). The third suggests
281   that the process is stopped before completion after a certain period, which we consider here for
282   simplicity. In all cases, the total amount of HEI10 loaded onto the SC determines the number
283   of CO-promoting droplets, although in the third case the length of the SC also plays a minor
284   role independently of the total amount of HEI10. The model proposes that two factors jointly
285   determine the initial HEI10 loading: (i) HEI10 concentration in the nucleoplasm, which
286   determines the amount of HEI10 in initial droplets and on the SC per μm of SC (ii) the length
287   of the SC, which, for a given expression level of HEI10 would determine linearly the total
288   HEI10 loading. Our numerical implementation of this model (see Methods) explains the
289   measured CO counts quantitatively (Figure 6A,B). In particular, it explains the observed
290   correlation between the length of the SC and the number of COs between chromosome pairs
291   within single cells as well as between different cells, as notably observed here in Arabidopsis,
292   where female meiosis has a shorter SC and fewer COs than male meiosis. Note that this shorter
293   SC in females also implies stronger CO interference (Figure 6C,F, G; compare with Figure 2).
294   This model also accounts for the fact that CO number depends on HEI10 expression level, as
295   this level determines the amount of HEI10 loaded per μm of SC. Remarkably, we observed
296   that overexpressing HEI10 increases CO numbers in males and females without eliminating
297   heterochiasmy, as predicted by the difference in SC length. In addition, CO interference is also
298   reduced, but not abolished by over-expressing HEI10, as expected, as the coarsening process
299   still occurs (Figure 6D,F,H, I). We propose that in the absence of SC, in the *zyp1* mutant, HEI10
300   diffusion is no longer constrained to the SC but occurs freely in the nucleoplasm. In this case,
301   droplets still form on chromosomes (Figure 1A-B), but they now exchange HEI10 directly with
302   the nucleoplasm. If this exchange is slow compared to the duration of pachytene, all initial
303   droplets grow continuously by taking up HEI10. In contrast, when HEI10 is exchanged more
304   quickly, competition between droplets, and thus coarsening, will set in, which was also recently
305   proposed[31]. In both cases, large HEI10 foci form, colocalize with MLH1, and promote class I
306   COs. However, the obligate CO and CO interference are lost as the diffusion is no longer
307   constrained per chromosome (Figure 6E,J). In a sense, in the absence of the SC, the coarsening
308   and CO designation process can be said to be "blind" to chromosomes. The absence of the SC
309   must be associated with slower coarsening since otherwise the exchange of HEI10 via the
310   nucleoplasm would be significant in wild type, too. If the number of initial droplets in the *zyp1*
311   mutant is roughly comparable to wild type, slower coarsening implies a bigger number of large
312   droplets at the end of pachytene, consistent with the increase observed experimentally (Figure

313   1). Together with interference, heterochiasmy is abolished when the number of COs per
314   chromosome is solely determined by HEI10 expression level in the nucleoplasm and no longer
315   by HEI10 loading onto the SC. Taken together, the experimental data and the coarsening model
316   show that two factors limit class I COs: ZYP1-mediated CO-interference and HEI10 levels.

317   A similar model was proposed and further supporting experimental data were recently obtained
318   in *C. elegans*[5]. Several additional pieces of evidences suggest that the dual control of COs by
319   SC and HEI10 is conserved: In multiple species, HEI10 homologs also initially form multiple
320   foci before eventually consolidating into a limited number of large foci that co-localize with
321   COs[19-22,32]; COs covary with SC length in many species[4]; Variants that affect recombination
322   rates in natural populations of diverse species involve genes that encode HEI10 homologues[33].
323   This suggests that the coarsening of HEI10 along the SC may be a conserved process for CO
324   patterning in eukaryotes.

Materials and methods

Plant Materials and Growth Conditions

Arabidopsis thaliana plants were cultivated in Polyklima growth chambers (16-h day, 21.5 °C, 280 µM; 8-h night, 18 °C: 60% humidity). Wild-type Col-0 and L*er*-1 are 186AV1B4 and 213AV1B1 from the Versailles stock center (http://publiclines.versailles.inra.fr/). The *zyp1-1* (8.7.2V1T3) and *zyp1-6* (1.12V5T2) mutants were previously described[11]. The HEI10 over-expression line is Col HEI10 line C2[23], kindly provided by Ian Henderson. Genotyping of the mutants was carried out by PCR amplification (Dataset S1).

To generate the double homozygous mutant *zyp1-1*$^{-/-}$ HEI10^{oe} in Col, *zyp1-1*$^{+/-}$ plants were crossed with HEI10^{oe} homozygous mutant plants (C2). The obtained double heterozygous *zyp1-1*$^{+/-}$ HEI10^{oe} were selfed to produce *zyp1-1*$^{-/-}$ mutants, HEI10^{oe} homozygous, and *zyp1-1*$^{-/-}$ HEI10^{oe} double homozygous mutants. These sister plants were used to perform MLH1 foci counting, SC measurements, chromosome spreads, and seed countings. To generate *zyp1-1/zyp1-6* HEI10$^{oe\ het}$ in Col/L*er*, double heterozygous *zyp1-1*$^{+/-}$ HEI10^{oe} (Col) were crossed with *zyp1-6*$^{+/-}$ (L*er*) to generate *zyp1-1/zyp1-6* HEI10$^{oe\ het}$, HEI10$^{oe\ het}$, *zyp1-1/zyp1-6* and wild-type controls in Col/L*er*. These sister plants were used for MLH1 foci counting and SC length measurements and were reciprocally backcrossed with wild-type Col to generate the sequencing populations. Backcross populations were grown in the greenhouse for three weeks (16-h day/8-h night) and four days in the dark. For DNA extraction and library preparation, 100–150mg leaf samples were collected from the four backcross populations [34].

Cytology

Chromosome spreads and immunolocalization of male meiocytes on 3D slides were conducted as previously described[35,11]. For female 3D slides, 0.8–1.2mm pistils were collected and their stigmata cut off. Pistils were then fixed and digested following the same procedure as for male meiocytes. The pistils were then opened longitudinally and the ovules released on a slide. The subsequent slide treatment and immunolocalization were the same as for male meiocytes, and were described previously[11].

Four primary antibodies were used: anti-REC8 raised in rat[36] (laboratory code PAK036, dilution 1:250), anti-MLH1 in rabbit[37] (PAK017, 1:200), anti-HEI10 in chicken[19] (PAK046,

354   1:5,000) and anti-ZYP1N in guinea pig[11] (PAK053, 1:500). Secondary antibodies were STAR

355   RED, STAR ORANGE and STAR GREEN, or Alexa488. Super-resolution images were

356   acquired with the Abberior instrument facility line (https://abberior-instruments.com/) 561-

357   and 640-nm excitation lasers (for STAR Orange and STAR Red, respectively) and a 775-nm

358   STED depletion laser. Confocal images were taken with the same instrument with a 485-nm

359   excitation laser (for STAR GREEN/Alexa488).

Image processing and analysis

361   Deconvolution of the images was performed by Huygens Essential (version 21.10, Scientific

362   Volume Imaging, https://svi.nl/) using the classic maximum likelihood estimation algorithm

363   with lateral drift stabilization; signal-to-noise ratio: 7 for STED images and 20 for confocal

364   images, 40 iterations, and quality threshold of 0.5. Maximum intensity projections and contrast

365   adjustments were also done with Huygens Essential. Deconvoluted pictures were imported into

366   Imaris 9.8 (https://imaris.oxinst.com/, Oxford Instruments, UK) for subsequent analysis.

367   MLH1 foci were counted using the spots module in diplotene and diakinesis cells. The vast

368   majority of MLH foci colocalize with a HEI10 focus. Only double MLH1/HEI10 foci present

369   on chromosomes were taken into account. For REC8 signal tracing, fully synapsed cells were

370   used to trace the chromosomes. In wild type and HEI10[oe], the five synapsed bivalents were

371   traced. In *zyp1* and *zyp1* HEI10[oe], five pairs of parallel chromosomes were traced. The surface

372   module was used to create a clean masked REC8 channel for filament tracing. The filament

373   module was used to trace the SC length, AutoDepth function was used to do semi-automatic

374   tracing and get the simulated chromosome. The SC length of each chromosome was measured

375   using the statistics function of the Filament module.

CO identification and analysis

377   In this study, the female and male population of wild type (48 and 47 plants), HEI10[oe] (144

378   and 141 plants), *zyp1* (48 and 47 plants) and *zyp1* HEI10[oe] (142 and 138 plants) were sequenced

379   by Illumina HiSeq3000 (2x150bp) conducted by the Max Planck-Genome-center

380   (https://mpgc.mpipz.mpg.de/home/). The raw sequencing data of the female and male

381   population of wild type (212 and 120 plants respectively) and *zyp1* (224 and 178 plants) from

382   a previous study (ArrayExpress number aE-MTAB-9593) [11] were also included in this study. In

383   total, we analyzed 260 and 167 wild type female and male, 144 and 141 HEI10[oe] female and

384   male, 272 and 225 *zyp1* female and male, 142 and 138 *zyp1* HEI10[oe] female and male plants,

385   separately. The raw sequencing data were quality-controlled using FastQC v0.11.9

386   (http://www.bioinformatics.babraham.ac.uk/projects/fastqc/). The sequencing reads were

387   aligned to the *Arabidopsis thaliana* Col-0 TAIR10 reference genome, which was downloaded

388   from TAIR [38,39], using BWA v0.7.15-r1140[40], with default parameters. A set of Sambamba

389   v0.6.8[41] commands was used for sorting and removing duplicated mapped reads. The creation

390   of the high-confidence SNP marker list between Col and L*er*, meiotic CO detection (a sliding

391   window-based method, with a window size of 50 kb and a step size of 25 kb), check and

392   filtering of low covered and potential contaminated samples were performed according to

393   previous protocols[11,27,42-44]. Samples of each population were randomly selected for checking

394   predicted COs manually by inGAP-family[43]. The Coefficient of Coincidence (CoC) was

395   calculated for CO interference analysis using MADpattern[45,46], with a number of 13 intervals.

396   Chromosome 4 was excluded from interference analyses. To profile the CO distribution along

397   chromosomes, CO position was defined randomly in the range of CO interval and a sliding

398   window-based strategy was used, with 1 Mb window size and 50 kb step size. Then, the local

399   distribution of recombination (CO resolution <= 1000 bp) was explored by ChIPseeker

400   v1.22.1[47], with the promoter region defined as 2000 bp upstream of the transcription start site.

401   **Aneuploidy screening by whole genome sequencing**

402   The sequencing depth of each non-overlapping 100 kb window across the genome was

403   evaluated by Mosdepth v0.2.7[48] with parameters of "-n --fast-mode --by 10000". For each

404   sample, pairwise testing of sequencing depths along chromosomes was performed using the

405   Mann-Whitney test, and significant p values were adjusted using the fdr method. A pair of

406   tested chromosomes with fold change > 1.2 and p value < 1e-20 was considered as aneuploid.

407   **Mathematical model of CO patterning**

408   Our mathematical model describes the concentration $c(x, t)$ of HEI10 along the SC of length

409   L together with the amounts $M_i(t)$ of HEI10 in N droplets that are placed at positions x_i along

410   the SC for $i = 1, ..., N$. Here, x denotes the length along the SC and t denotes time. Similar to

411   the model presented in ref.[6], we account for the diffusion of HEI10 along the SC and the

412   exchange of HEI10 between SC and droplets. Droplet i grows if the local HEI10 concentration

413   on the SC, $c(x_i)$, is larger than the equilibrium concentration $c^{eq}(M_i) = c_0^{eq} \frac{M_i}{1+M_i^{1+\alpha}}$,

414
$$\frac{dM_i}{dt} = \Lambda[c(x_i) - c^{\text{eq}}(M_i)]$$

415 where Λ quantifies the rate of HEI10 exchange. HEI10 diffuses with diffusivity D along the
416 SC and is exchanged with droplets,

417
$$\frac{\partial c}{\partial t} = D\frac{\partial^2 c}{\partial x^2} - \Lambda\sum_{i=1}^{N}\delta(x - x_i)[c(x_i) - c^{\text{eq}}(M_i)]$$

418 We impose no-flux boundary conditions at $x = 0$ and $x = L$, so the total amount of HEI10 is
419 conserved. We implemented this model using finite differences by discretizing the SC using
420 50 grid points and solved the resulting equations using an explicit Euler scheme.

421 We initialize the system with a uniform concentration on the SC, $c(x, t = 0) = c_{\text{init}}$. The N
422 droplets are positioned uniformly along the SC and their sizes M_i are chosen independently
423 from a normal distribution with mean M_{init} and standard deviation σ, which has been truncated
424 to $[M_{\text{init}} - 3\sigma, M_{\text{init}} + 3\sigma]$. The diffusivity $D = 1.1\ \mu\text{m}^2/\text{s}$, the exchange rate $\Lambda = 2.1\ \mu\text{m}/\text{s}$,
425 the exponent $\alpha = 0.25$, and the base equilibrium concentration $c_0^{\text{eq}} = 1.35\ \text{a.u.}/\mu\text{m}$, are
426 inspired by ref.[6]. We use SC lengths L measured in wild type (Figure 4N) and estimate an initial
427 droplet density of four droplets per μm, based on cytology[49]. For simulations, we choose
428 $M_{\text{init}} = y \cdot 3.4\ \text{a.u.}$, $\sigma_{\text{init}} = y \cdot 1.1\ \text{a.u.}$, and $c_{\text{init}} = y \cdot 1.4\ \text{a.u.}/\mu\text{m}$, where y is a factor to
429 account for higher HEI10 expression levels. We chose $y = 2$ for wild type Col, $y = 6$ for
430 HEI10[oe het] Col, $y = 8$ for HEI10[oe homo] Col, $y = 1.5$ for wild type Col/L*er*, and $y = 5.5$ for
431 HEI10[oe het] Col/L*er*, which accounts for the reduced activity in L*er*[50] and HEI10
432 overexpression. We simulate droplet coarsening on each individual SC for male and female
433 meiosis for 10h, comparable to the duration of pachytene[51,52]. Only droplets above a threshold
434 size of $M_{\text{thresh}} = 3\ \text{a.u.}$ are assumed to attract MLH1 and form class I COs. The associated COs
435 per chromatid were determine by choosing COs from the bivalent independently with 50%
436 probability.

437 In the case of the *zyp1* mutant, our model implies that all CO positions are independent. To
438 obtain a theoretical distribution of COs, we thus first determine the number of COs per
439 chromatid by sampling a Poisson distribution with a mean given by the experimental data
440 (Figure 4N) and then distribute these COs uniformly along the chromatid length.

Data Availability

MLH1 counts and SC length measurements are shown in table S1 and S6, respectively. The raw sequencing data is deposited in ArrayExpress of EMBL-EBI with accession numbers E-MTAB-11696. The list of identified COs in the female and male populations of wild type, HEI10^{oe}, *zyp1*, and *zyp1* HEI10^{oe} can be accessed in Supplemental Table S2-S5.

Author contributions

S.D. produced and analyzed the MLH1-HEI10 cytological data, developed the protocol for female immunolocalization, produced all the genetic material, and analyzed fertility. Q.L. analyzed the sequencing data and performed recombination, interference, and aneuploidy analyses. J.J. generated SC images, and analyzed chromosome missegregation and SC length data. M.E. and D.Z. developed the mathematical model of CO patterning. M.G. developed the method for chromosome 3D analyses. R.M. lead the project and wrote the manuscript with input from all co-authors.

Supplementary Information is available for this paper

Correspondence and requests for materials should be addressed to Raphael Mercier

References

1   Otto, S. P. & Payseur, B. A. Crossover Interference: Shedding Light on the Evolution of Recombination. *Annual Review of Genetics* **53**, 19-44, doi:10.1146/annurev-genet-040119-093957 (2019).

2   Pyatnitskaya, A., Borde, V., De Muyt, A. & Crossing and zipping: molecular duties of the ZMM proteins in meiosis. *Chromosoma* **128**, 181-198, doi:10.1007/s00412-019-00714-8 (2019).

3   von Diezmann, L. & Rog, O. Let's get physical - mechanisms of crossover interference. *J Cell Sci* **134**, doi:10.1242/jcs.255745 (2021).

4   Kleckner, N., Storlazzi, A. & Zickler, D. Coordinate variation in meiotic pachytene SC length and total crossover/chiasma frequency under conditions of constant DNA length. *Trends in Genetics* **19**, 623-628, doi:https://doi.org/10.1016/j.tig.2003.09.004 (2003).

5   Zhang, L., Stauffer, W., Zwicker, D. & Dernburg, A. F. Crossover patterning through kinase-regulated condensation and coarsening of recombination nodules. *bioRxiv*, 2021.2008.2026.457865, doi:10.1101/2021.08.26.457865 (2021).

6   Morgan, C. *et al.* Diffusion-mediated HEI10 coarsening can explain meiotic crossover positioning in Arabidopsis. *Nat Commun* **12**, 4674, doi:10.1038/s41467-021-24827-w (2021).

7   Sturtevant, A. H. The linear arrangement of six sex-linked factors in Drosophila, as shown by their mode of association. *J Exp Zool* **14**, 43-59, doi:DOI 10.1002/jez.1400140104 (1913).

8   Sturtevant, A. H. The behavior of the chromosomes as studied through linkage. *Zeitschrift für induktive Abstammungs- und Vererbungslehre* **13**, 234-287, doi:10.1007/BF01792906 (1915).

9   Zickler, D. & Kleckner, N. A few of our favorite things: Pairing, the bouquet, crossover interference and evolution of meiosis. *Seminars in Cell & Developmental Biology* **54**, 135-148, doi:https://doi.org/10.1016/j.semcdb.2016.02.024 (2016).

10   France Martin, G. *et al.* ZYP1 is required for obligate cross-over formation and cross-over interference in Arabidopsis. *Proceedings of the National Academy of Sciences* **118**, e2021671118, doi:10.1073/pnas.2021671118 (2021).

11   Capilla-Pérez, L. *et al.* The synaptonemal complex imposes crossover interference and heterochiasmy in. *Proceedings of the National Academy of Sciences* **118**, e2023613118, doi:10.1073/pnas.2023613118 (2021).

12   Libuda, D. E., Uzawa, S., Meyer, B. J. & Villeneuve, A. M. Meiotic chromosome structures constrain and respond to designation of crossover sites. *Nature* **502**, 703-706, doi:10.1038/nature12577 (2013).

13   Gordon, S. G., Kursel, L. E., Xu, K. & Rog, O. Synaptonemal Complex dimerization regulates chromosome alignment and crossover patterning in meiosis. *PLOS Genetics* **17**, e1009205, doi:10.1371/journal.pgen.1009205 (2021).

14   Voelkel-Meiman, K., Cheng, S.-Y., Morehouse, S. J. & MacQueen, A. J. Synaptonemal Complex Proteins of Budding Yeast Define Reciprocal Roles in MutSγ-Mediated Crossover Formation. *Genetics* **203**, 1091-1103, doi:10.1534/genetics.115.182923 (2016).

15   Voelkel-Meiman, K. *et al.* Crossover recombination and synapsis are linked by adjacent regions within the N terminus of the Zip1 synaptonemal complex protein. *PLOS Genetics* **15**, e1008201, doi:10.1371/journal.pgen.1008201 (2019).

16   Drouaud, J. *et al.* Sex-Specific Crossover Distributions and Variations in Interference Level along Arabidopsis thaliana Chromosome 4. *PLOS Genetics* **3**, e106, doi:10.1371/journal.pgen.0030106 (2007).

17   Shang, Y. *et al.* Meiotic chromosome organization and crossover patterns†. *Biology of Reproduction*, ioac040, doi:10.1093/biolre/ioac040 (2022).

18   Lloyd, A. & Jenczewski, E. Modelling Sex-Specific Crossover Patterning in Arabidopsis. *Genetics* **211**, 847-859, doi:10.1534/genetics.118.301838 (2019).

19   Chelysheva, L. *et al.* The Arabidopsis HEI10 is a new ZMM protein related to Zip3. *PLoS Genet* **8**, e1002799, doi:10.1371/journal.pgen.1002799 (2012).

515 20 Dubois, E. *et al.* Building bridges to move recombination complexes. *Proceedings of the National Academy of Sciences* **116**, 12400-12409, doi:10.1073/pnas.1901237116 (2019).

517 21 Wang, K. *et al.* The Role of Rice HEI10 in the Formation of Meiotic Crossovers. *PLOS Genetics* **8**, e1002809, doi:10.1371/journal.pgen.1002809 (2012).

519 22 Qiao, H. *et al.* Antagonistic roles of ubiquitin ligase HEI10 and SUMO ligase RNF212 regulate meiotic recombination. *Nat Genet* **46**, 194-199, doi:10.1038/ng.2858 (2014).

521 23 Ziolkowski, P. A. *et al.* Natural variation and dosage of the HEI10 meiotic E3 ligase control Arabidopsis crossover recombination. *Genes Dev* **31**, 306-317, doi:10.1101/gad.295501.116 (2017).

524 24 Jiao, W.-B. & Schneeberger, K. Chromosome-level assemblies of multiple Arabidopsis genomes reveal hotspots of rearrangements with altered evolutionary dynamics. *Nature Communications* **11**, 989, doi:10.1038/s41467-020-14779-y (2020).

527 25 Zapata, L. *et al.* Chromosome-level assembly of Arabidopsis thaliana Ler reveals the extent of translocation and inversion polymorphisms. *Proceedings of the National Academy of Sciences* **113**, E4052-E4060, doi:10.1073/pnas.1607532113 (2016).

530 26 Wang, S. *et al.* Per-Nucleus Crossover Covariation and Implications for Evolution. *Cell* **177**, 326-338, doi:10.1016/j.cell.2019.02.021 (2019).

532 27 Lian, Q. *et al.* The megabase-scale crossover landscape is independent of sequence divergence. *bioRxiv*, 2022.2001.2010.474936, doi:10.1101/2022.01.10.474936 (2022).

534 28 Fernandes, J. B., Séguéla-Arnaud, M., Larchevêque, C., Lloyd, A. H. & Mercier, R. Unleashing meiotic crossovers in hybrid plants. *Proceedings of the National Academy of Sciences* **115**, 2431-2436, doi:10.1073/pnas.1713078114 (2018).

537 29 Séguéla-Arnaud, M. *et al.* Multiple mechanisms limit meiotic crossovers: TOP3α and two BLM homologs antagonize crossovers in parallel to FANCM. *Proc Natl Acad Sci U S A* **112**, 4713-4718, doi:10.1073/pnas.1423107112 (2015).

540 30 Crismani, W. *et al.* FANCM limits meiotic crossovers. *Science* **336**, 1588-1590, doi:10.1126/science.1220381 (2012).

542 31 Fozard, J. A., Morgan, C. & Howard, M. The synaptonemal complex controls cis- versus trans-interference in coarsening-based meiotic crossover patterning. *bioRxiv*, 2022.2004.2011.487855, doi:10.1101/2022.04.11.487855 (2022).

545 32 Lake, C. M. *et al.* Vilya, a component of the recombination nodule, is required for meiotic double-strand break formation in Drosophila. *Elife* **4**, e08287, doi:10.7554/eLife.08287 (2015).

548 33 Stapley, J., Feulner, P. G. D., Johnston, S. E., Santure, A. W. & Smadja, C. M. Variation in recombination frequency and distribution across eukaryotes: patterns and processes. *Philosophical transactions of the Royal Society of London. Series B, Biological sciences* **372**, doi:10.1098/rstb.2016.0455 (2017).

552 34 Rowan, B. A., Patel, V., Weigel, D. & Schneeberger, K. Rapid and Inexpensive Whole-Genome Genotyping-by-Sequencing for Crossover Localization and Fine-Scale Genetic Mapping. *G3 Genes|Genomes|Genetics* **5**, 385-398, doi:10.1534/g3.114.016501 (2015).

555 35 Cromer, L. *et al.* Patronus is the elusive plant securin, preventing chromosome separation by antagonizing separase. *Proc Natl Acad Sci U S A* **116**, 16018-16027, doi:10.1073/pnas.1906237116 (2019).

558 36 Cromer, L. *et al.* Centromeric Cohesion Is Protected Twice at Meiosis, by SHUGOSHINs at Anaphase I and by PATRONUS at Interkinesis. *Current Biology* **23**, 2090-2099, doi:https://doi.org/10.1016/j.cub.2013.08.036 (2013).

561 37 Chelysheva, L. *et al.* An Easy Protocol for Studying Chromatin and Recombination Protein Dynamics during Arabidopsis thaliana Meiosis: Immunodetection of Cohesins, Histones and MLH1. *Cytogenetic and genome research* **129**, 143-153, doi:10.1159/000314096 (2010).

564 38 Lamesch, P. *et al.* The Arabidopsis Information Resource (TAIR): improved gene annotation and new tools. *Nucleic Acids Research* **40**, D1202-D1210, doi:10.1093/nar/gkr1090 (2012).

566 39   The Arabidopsis Genome, I. Analysis of the genome sequence of the flowering plant
567   Arabidopsis thaliana. *Nature* **408**, 796-815, doi:10.1038/35048692 (2000).
568 40   Li, H. & Durbin, R. Fast and accurate short read alignment with Burrows–Wheeler transform.
569   *Bioinformatics* **25**, 1754-1760, doi:10.1093/bioinformatics/btp324 (2009).
570 41   Tarasov, A., Vilella, A. J., Cuppen, E., Nijman, I. J. & Prins, P. Sambamba: fast processing of
571   NGS alignment formats. *Bioinformatics* **31**, 2032-2034, doi:10.1093/bioinformatics/btv098
572   (2015).
573 42   Qi, J., Chen, Y., Copenhaver Gregory, P. & Ma, H. Detection of genomic variations and DNA
574   polymorphisms and impact on analysis of meiotic recombination and genetic mapping.
575   *Proceedings of the National Academy of Sciences* **111**, 10007-10012,
576   doi:10.1073/pnas.1321897111 (2014).
577 43   Lian, Q., Chen, Y., Chang, F., Fu, Y. & Qi, J. inGAP-family: Accurate Detection of Meiotic
578   Recombination Loci and Causal Mutations by Filtering Out Artificial Variants due to Genome
579   Complexities. *Genomics, Proteomics & Bioinformatics*,
580   doi:https://doi.org/10.1016/j.gpb.2019.11.014 (2021).
581 44   Wang, H. *et al.* The cohesin loader SCC2 contains a PHD finger that is required for meiosis in
582   land plants. *PLOS Genetics* **16**, e1008849, doi:10.1371/journal.pgen.1008849 (2020).
583 45   Zhang, L., Liang, Z., Hutchinson, J. & Kleckner, N. Crossover Patterning by the Beam-Film
584   Model: Analysis and Implications. *PLOS Genetics* **10**, e1004042,
585   doi:10.1371/journal.pgen.1004042 (2014).
586 46   White, M. A., Wang, S., Zhang, L. & Kleckner, N. in *Meiosis* (ed David T. Stuart) 305-323
587   (Springer New York, 2017).
588 47   Yu, G., Wang, L.-G. & He, Q.-Y. ChIPseeker: an R/Bioconductor package for ChIP peak
589   annotation, comparison and visualization. *Bioinformatics* **31**, 2382-2383,
590   doi:10.1093/bioinformatics/btv145 (2015).
591 48   Pedersen, B. S. & Quinlan, A. R. Mosdepth: quick coverage calculation for genomes and
592   exomes. *Bioinformatics* **34**, 867-868, doi:10.1093/bioinformatics/btx699 (2018).
593 49   Capilla-Pérez, L. *et al.* The synaptonemal complex imposes crossover interference and
594   heterochiasmy in Arabidopsis. *Proc. Natl. Acad. Sci. USA* **118**, e2023613118,
595   doi:10.1073/pnas.2023613118 (2021).
596 50   Ziolkowski, P. A. *et al.* Natural variation and dosage of the HEI10 meiotic E3 ligase control
597   Arabidopsis crossover recombination. *Genes & Development* (2017).
598 51   Armstrong, S. J., Franklin, F. C. H. & Jones, G. H. A meiotic time-course for Arabidopsis
599   thaliana. *Sex. Plant Reprod.* **16**, 141--149, doi:10.1007/s00497-003-0186-4 (2003).
600 52   Prusicki, M. A. *et al.* Live cell imaging of meiosis in Arabidopsis thaliana. *eLife* **8**, e42834,
601   doi:10.7554/eLife.42834 (2019).
602 53   Serra, H. *et al.* Massive crossover elevation via combination of HEI10 and recq4a recq4b
603   during Arabidopsis meiosis. *Proc Natl Acad Sci U S A* **115**, 2437-2442,
604   doi:10.1073/pnas.1713071115 (2018).

605

606

Figure legends

Figure 1. Massive increase in crossovers through combination of *zyp1* mutation and HEI10 overexpression

610 (A) MLH1 foci in Col wild type and *zyp1* HEI10$^{oe\ homo}$ meiocytes. Following
611 immunolocalization, REC8 (Purple) and HEI10 (not shown) were imaged with STED while
612 MLH1 (green) was imaged with confocal microscopy. The maximum intensity projection is
613 shown. Scale bar=1μm. (B) Corresponding MLH1 foci quantification, in female and male,
614 inbred Col and hybrid Col/L*er*. The HEI10 transgene originates from the C2 line and is either
615 homozygous (HEI10$^{oe\ het}$) or heterozygous (HEI10$^{oe\ homo}$). Each dot is an individual cell, and
616 the mean is indicated by a bar and a number on the top. (C) Experimental design for
617 construction of female and male hybrid populations for sequencing. (D) The number of COs
618 per gamete in female and male populations of wild type, HEI10^{oe}, *zyp1*, and *zyp1* HEI10^{oe}.
619 Each point is a BC1/gamete, and the means are indicated by horizontal dashed lines and
620 numbers on the top. The population size is shown in parentheses. (E) Correlation analysis
621 between mean number of COs per chromosome per gamete and chromosome size (Mb). Error
622 bars are the 90% confidence intervals of the mean. Pearson's correlation coefficients are shown
623 in parentheses. (F) Chromosomal genotypes are shown for representative gametes for wild type
624 and mutants, and for extreme cases for *zyp1* HEI10^{oe} populations. Centromere positions are
625 indicated by white points.

626

627 **Figure 2. CO distribution and interference analysis in female and male wild type,**
628 **HEI10^{oe}, *zyp1*, and *zyp1* HEI10^{oe}.**

629 (A–B) The distribution of COs on chromosome 1 in (A) female and (B) male of wild type,
630 HEI10^{oe}, *zyp1*, and *zyp1* HEI10^{oe}. The other chromosomes are shown in Figure S3. (C–F)
631 Distribution of distances between two COs for chromosomes with exactly two COs (Figure
632 S5). The grey bar represents the expected distribution of COs without interference, calculated
633 by permutation analysis of COs. The number of analyzed CO pairs and the p-value from the
634 Mann-Whitney test between the expected and observed are indicated. (G-J) CoC curves in
635 female and male meiosis of wild type, HEI10^{oe}, *zyp1*, and *zyp1* HEI10^{oe}, respectively.
636 Chromosomes were divided into 13 intervals, for calculating the mean coefficient of
637 coincidence of each pair of intervals.

638

639 **Figure 3. Analysis of meiotic and fertility defects**

640   (A–F) DAPI-stained meiotic chromosome spreads from Col/Ler male meiocytes in wild type

641   (A, B) and *zyp1* HEI10^{oe} (C-F). (A, C, E) Metaphase I. (B, D, F) Metaphase II. (C, D) Normal

642   chromosome configurations in *zyp1* HEI10^{oe}. (E, F) Rare abnormal chromosome

643   configurations in *zyp1* HEI10^{oe}. Scale bar=10μm. (G–H) Representative cleared fruits of wild-

644   type Col and *zyp1* HEI10^{oe} mutants. (I) Corresponding quantification of fertility. Each dot

645   represents the fertility of an individual plant, measured as the number of seeds per fruits

646   averaged on ten fruits. The red bar shows the mean. All plants were siblings grown together in

647   a growth chamber. *P* values are one-way ANOVA followed by Fisher's LSD test. (J) The

648   percentage of aneuploid samples detected in each population (Figure S6-7). The proportion of

649   aneuploid samples in each population is shown on top of the bars.

650

651   **Figure 4. Analysis of SC/axis lengths in female and male meiocytes**

652   (A–D) REC8 immunolocalization in female and male meiocytes of wild type and *zyp1* HEI10^{oe}

653   ^{homo} (Col). Imaging was done with 3D-STED and the projection is shown. Scale bar=1μm. (E–

654   H) REC8 signal was traced in 3D. Each bivalent pair is color-coded. (I–L) Individual trace of

655   the longest chromosome (presumably chromosome 1), with start-to-end color code. (M)

656   Measurement of the total SC length. Each dot is the SC length of an individual cell. The bars

657   indicate the mean. One-way ANOVA followed by Sidak correction showed that SCs were

658   systematically longer in males than in females (p < 0.0001). The same test did not detect any

659   differences between any of the pairs of males of different genotypes (p>0.4). For females, none

660   of the pairwise comparisons were significantly different except in Col/Ler HEI10^{oe} that was

661   lower than Col/Ler *zyp1* (p=0.006) and Col *zyp1* (p=0.008). Note that variations in slide

662   preparation and exact meiotic stage may affect this result. (N) Correlation analysis between the

663   mean number of COs per chromosome per gamete and SC length (μm) in Col/Ler background.

664   SCs were attributed to specific chromosomes based on their length (e.g., the longest was

665   presumably chromosome 1). Pearson's correlation coefficients are shown in parentheses. (O–

666   P) The relationship between the mean number of MLH1 foci per cell and total SC length per

667   cell in (O) Col background and (P) Col/Ler background. (Q) The relationship between the

668   mean number of COs per gamete and SC length in Col/Ler background. The 90% confidence

669   intervals are indicated as error bars.

670   **Figure 5. Model of crossover patterning *via* HEI10 coarsening**

671   HEI10 (red) is captured by the central element of the SC and coarsens into large pro-CO

672   droplets. The number of large pro-CO droplets is determined by SC length (heterochiasmy),

673   and HEI10 expression levels. HEI10 overexpression increases CO number, and weakens

674   interference but maintains heterochiasmy. In absence of an SC (*zyp1*), HEI10 is exchanged

675   directly between the droplets and the nucleoplasm abolishing both interference and

676   heterochiasmy, and the number of droplets depends on HEI10 expression level. Created with

677   BioRender.com

678

679   **Figure 6. A coarsening model for crossover designation explains the measured data**

680   (A) Number of MLH1 foci predicted by the model compared to the experimental measurements

681   shown in Figure 1B. Error bars denote 90% confidence. (B) Number of COs per chromatid

682   predicted by our model compared to the experimental measurements shown in Figure 1D. The

683   respective chromatids are labeled and error bars denote 90% confidence. (C–E) Predicted

684   coefficient of coincidence curves; compare to Figure 2G–J. (F–J) Predicted distributions of

685   distances between two COs for chromosomes with exactly two COs; compare to Figure 2C–F.

686   (A–J) Numerical details are given in the Methods. Mean and confidence intervals were

687   determined from $n = 1000$ (except $n = 500$ in panel A) independent repetitions.

688

689   **Supplemental Figure legends**

690   **Figure S1. Comparison of CO numbers between previous studies and this work.**

691   The number of COs per gamete in female and male populations of wild type and *zyp1*,
692   respectively. Different genotypes and studies are indicated through different colors and shapes,
693   respectively. The mean CO number of the population and significant *p* value (Mann-Whitney
694   test) are indicated in the top parentheses, with the same color codes.

695

696   **Figure S2. Correlation analysis of CO numbers between chromosomes.**

697   Pearson's correlation analysis of CO numbers between chromosomes in the same gamete was
698   performed in female and male populations of wild type, HEI10[oe], *zyp1*, and *zyp1* HEI10[oe]
699   individually. The sum of COs detected on chromosomes 1 and 2 was plotted against the sum
700   of COs on chromosomes 3 and 5 in the same gamete. A jitter function was applied to avoid
701   points overlapping. The correlation coefficients are shown in parentheses. The very low
702   correlation is in contrast with observations in several other species[26] and may be due to lower
703   cell-to-cell variation in Arabidopsis.

704

705   **Figure S3. The distribution of CO frequency along chromosomes.**

706   Comparison of CO distributions (sliding window-based, with window size of 1 Mb and step
707   size of 50 kb) between female and male of wild type (A), HEI10[oe] (B), *zyp1* (C) and *zyp1*
708   HEI10[oe] (D). Comparison of CO distribution among populations in female (E) and male (F)
709   meiosis. The pericentromeric and centromeric regions are indicated by grey and blue shading,
710   respectively. Consistent with previous observations[11,53], there is a ~2.2 Mb region on the long
711   arm of chromosome 4 where recombination is suppressed, which suggests a structural
712   arrangement between the Col and L*er* strains.

713

714   **Figure S4. The fine-scale distribution of COs.**

715   (A) The distribution of the length of CO intervals across populations. The length of 1 kb and 2

716   kb are indicated by grey dashed lines. The number of analyzed COs is shown in parentheses.

717   The median of CO intervals is 819 bp (B) The distribution of proportion of COs with interval

718   lengths less than 1 kb (high-resolution), more than 2 kb, and the rest separately. (C) The

719   distribution of proportion of high-resolution COs overlapping with genomic features. The

720   promoter region is defined as the 2 kb upstream of the transcription start site. The proportion

721   of the different genomic features is shown as the bar on the top, which is defined by following

722   the priority of promoter, 5' UTR, 3' UTR, exon, intron, and intergenic regions. (D) The

723   distribution of distance of high-resolution COs from nearest TSS.

724

725   **Figure S5. The distribution of positions of double-COs.**

726   Relative position of COs for chromosomes with exactly two COs (as in figure 2C-F). The

727   position of the first and second CO of the pair, in female and male meiosis of wild type,

728   HEI10^{oe}, *zyp1*, and *zyp1* HEI10^{oe}, respectively.

729

730   **Figure S6. The analysis of sequencing depths along chromosomes for aneuploidy**

731   **screening.**

732   The sequencing depth was calculated for each 100 kb non-overlapped interval along

733   chromosomes. The Mann-Whitney test was used for checking the differences between pairs of

734   chromosomes, the significant p value was then adjusted by the fdr method. The identity of the

735   detected aneuploidy is shown with the same color codes as for the corresponding populations.

736

737   **Figure S7. Sequencing depth along aneuploid chromosomes.**

738   The sequencing depth was calculated for each 100 kb non-overlapped interval along

739   chromosomes. The pericentromeric and centromeric regions are indicated by grey and blue

740   shading, respectively. The horizontal dashed line indicates the mean sequencing depth of the

741   sample. Aneuploidy is visible by higher coverage of one chromosome compared to the others.

742   The label of the detected aneuploidy and corresponding populations are presented individually.

743

744   **Table S1. Raw data of MLH1 counts.**

745   **Table S2. CO positions in wild-type population.**

746   **Table S3. CO positions in HEI10oe population.**

747   **Table S4. CO positions in *zyp1* population.**

748   **Table S5. CO positions in *zyp1* HEI10oe population.**

749   **Table S6. Raw data of SC Lengths.**

750   **Table S7. Summary data for mean MLH1 foci number, CO number, and SC length.**

751   **Table S8. Genotyping primers**
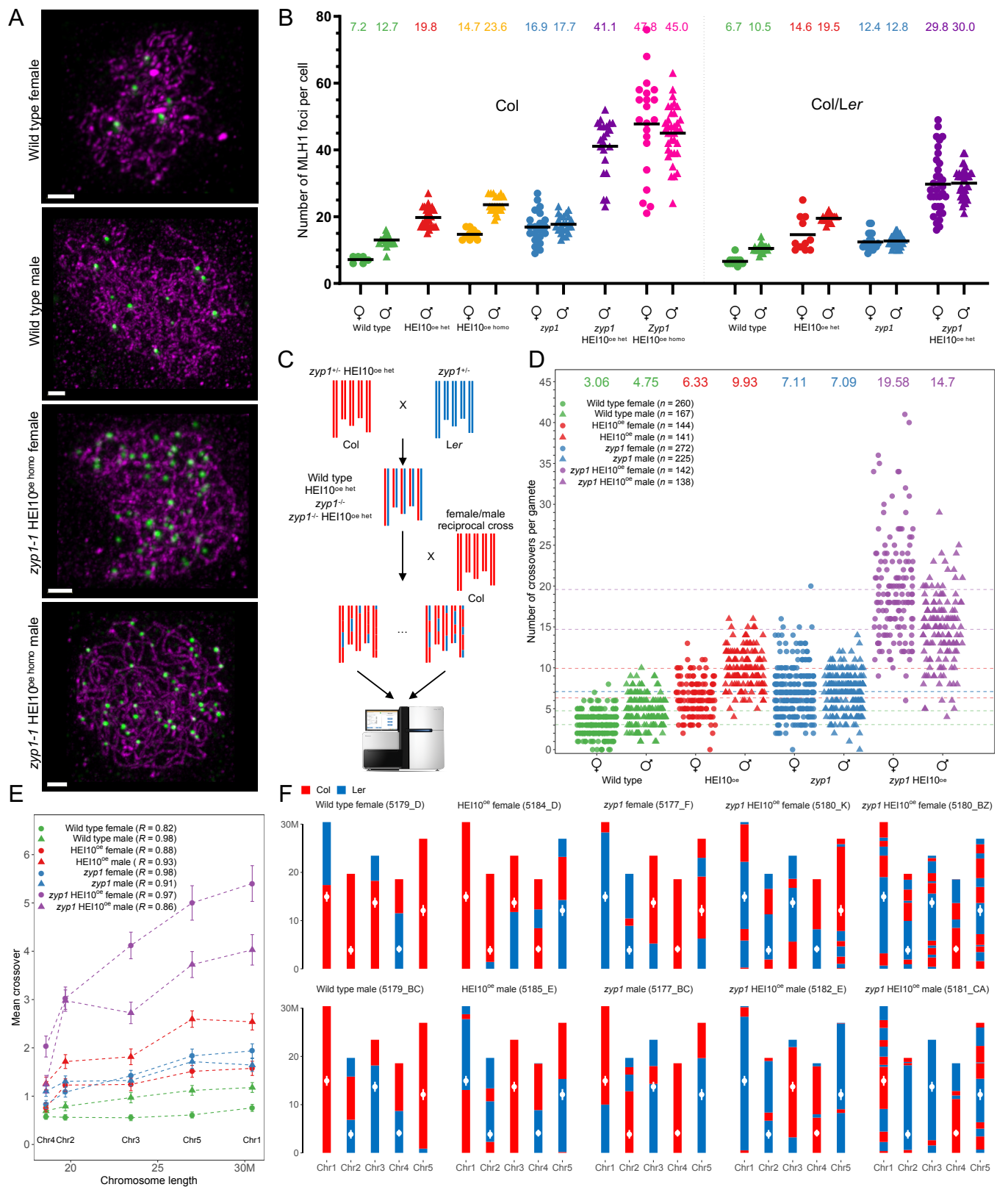
Figure 1. Massive increase in crossovers through combination of *zyp1* mutation and HEI10 overexpression

(A) MLH1 foci in Col wild type and *zyp1* HEI10[oe homo] meiocytes. Following immunolocalization, REC8 (Purple) and HEI10 (not shown) were imaged with STED while MLH1 (green) was imaged with confocal microscopy. The maximum intensity projection is shown. Scale bar=1μm. (B) Corresponding MLH1 foci quantification, in female and male, inbred Col and hybrid Col/L*er*. The HEI10 transgene originates from the C2 line and is either homozygous (HEI10[oe het]) or heterozygous (HEI10[oe homo]). Each dot is an individual cell, and the mean is indicated by a bar and a number on the top. (C) Experimental design for construction of female and male hybrid populations for sequencing. (D) The number of COs per gamete in female and male populations of wild type, HEI10[oe], *zyp1*, and *zyp1* HEI10[oe]. Each point is a BC1/gamete, and the means are indicated by horizontal dashed lines and numbers on the top. The population size is shown in parentheses. (E) Correlation analysis between mean number of COs per chromosome per gamete and chromosome size (Mb). Error bars are the 90% confidence intervals of the mean. Pearson's correlation coefficients are shown in parentheses. (F) Chromosomal genotypes are shown for representative gametes for wild type and mutants, and for extreme cases for *zyp1* HEI10[oe] populations. Centromere positions are indicated by white points.
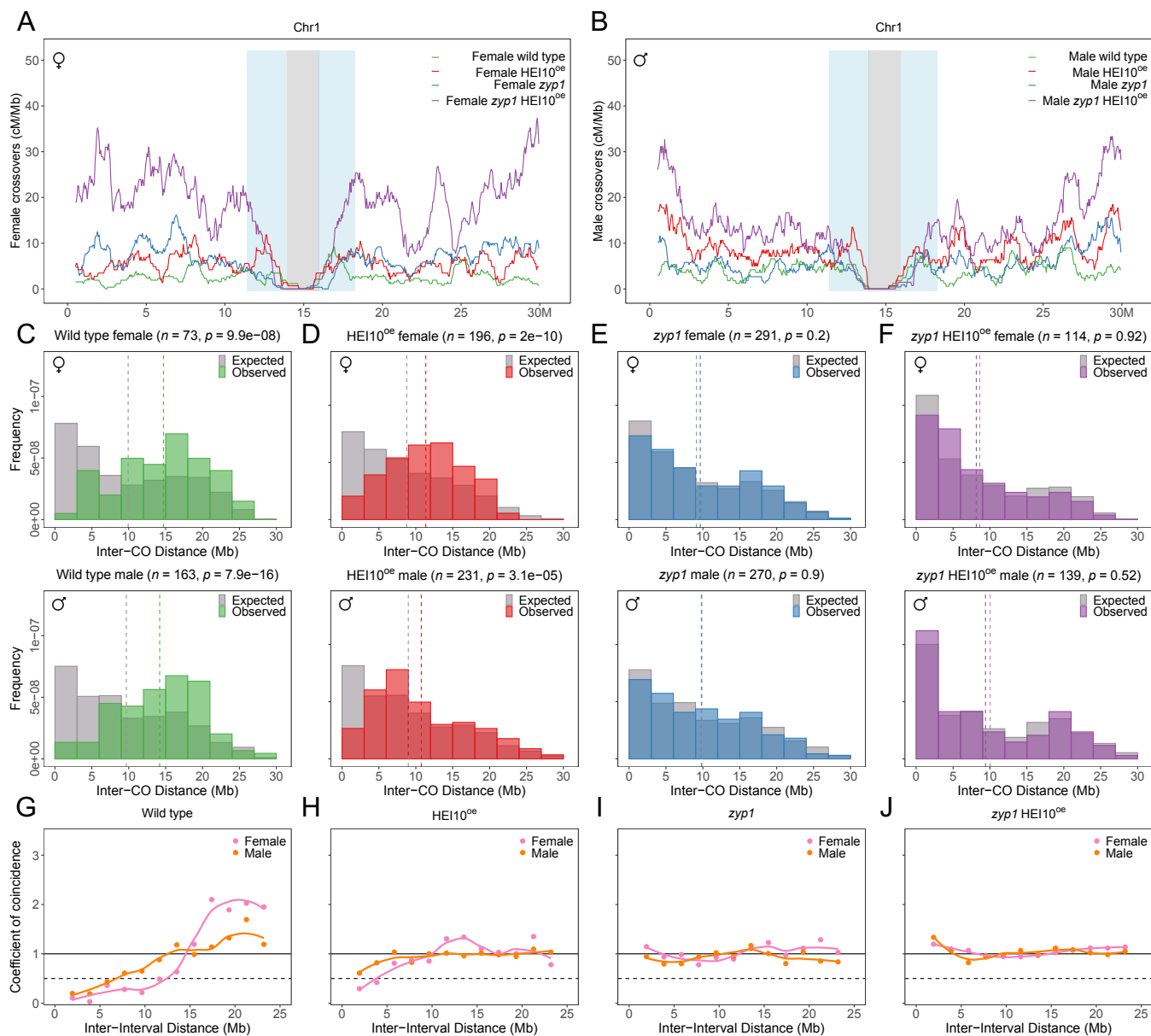
Figure 2. CO distribution and interference analysis in female and male wild type, HEI10oe, *zyp1*, and *zyp1* HEI10oe.

(A–B) The distribution of COs on chromosome 1 in (A) female and (B) male of wild type, HEI10oe, *zyp1*, and *zyp1* HEI10oe. The other chromosomes are shown in Figure S3. (C–F) Distribution of distances between two COs for chromosomes with exactly two COs. The grey bar represents the expected distribution of COs without interference, calculated by permutation analysis of COs. The number of analyzed CO pairs and the p-value from the Mann-Whitney test between the expected and observed are indicated.. (G-J) CoC curves in female and male meiosis of wild type, HEI10oe, *zyp1*, and *zyp1* HEI10oe, respectively. Chromosomes were divided into 13 intervals, for calculating the mean coefficient of coincidence of each pair of intervals.
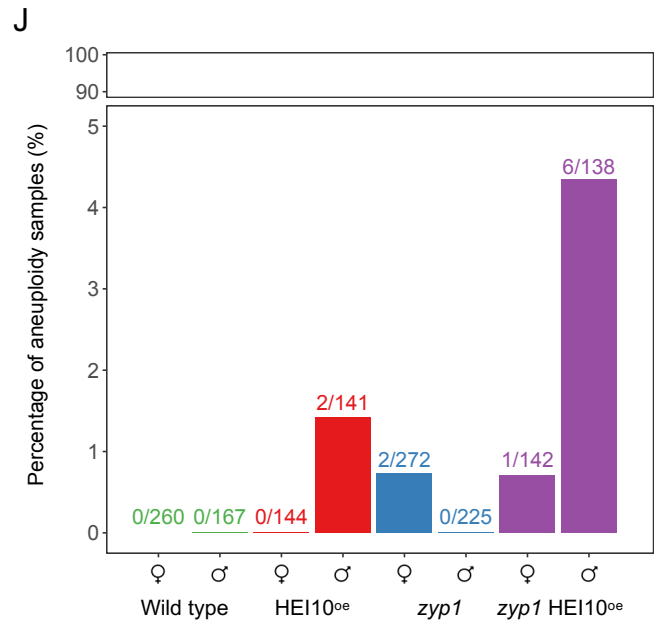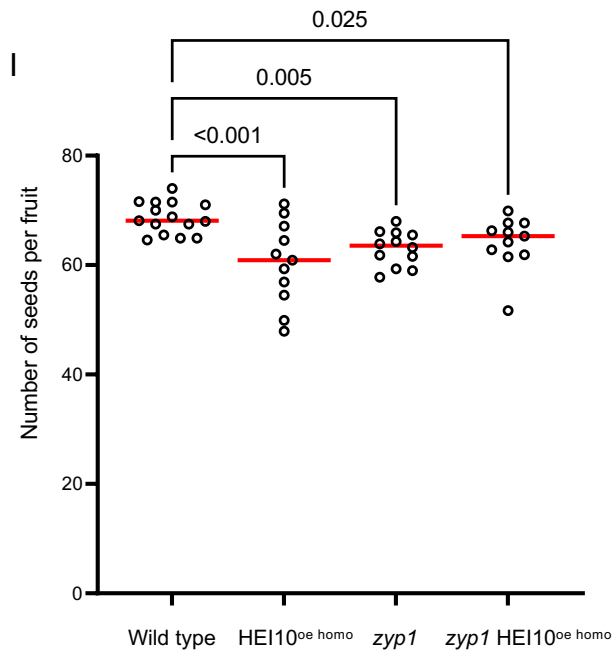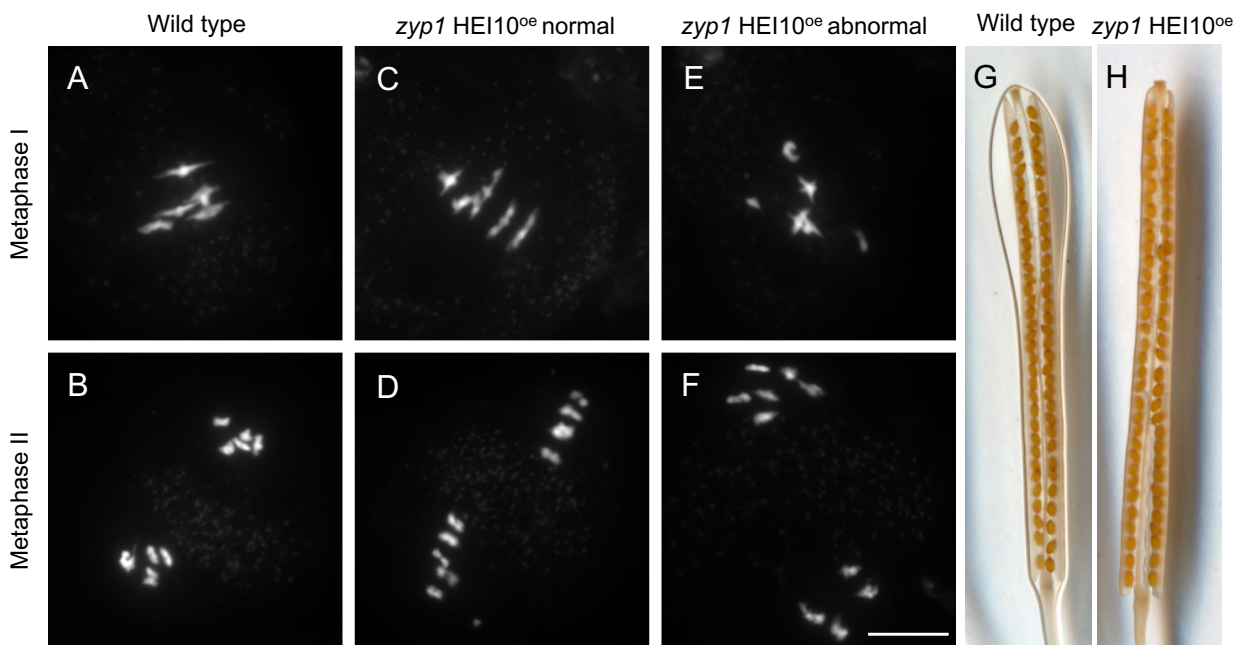
Figure 3. Analysis of meiotic and fertility defects

(A–F) DAPI-stained meiotic chromosome spreads from Col/L*er* male meiocytes in wild type (A, B) and *zyp1* HEI10oe (C-F). (A, C, E) Metaphase I. (B, D, F) Metaphase II. (C, D) Normal chromosome configurations in *zyp1* HEI10oe. (E, F) Rare abnormal chromosome configurations in *zyp1* HEI10oe. Scale bar=10μm. (G–H) Representative cleared fruits of wild-type Col and *zyp1* HEI10oe mutants. (I) Corresponding quantification of fertility. Each dot represents the fertility of an individual plant, measured as the number of seeds per fruits averaged on tenfruits. The red bar shows the mean. All plants were siblings grown together in a growth chamber. *P* values are one-way ANOVA followed by Fisher's LSD test. (J) The percentage of aneuploid samples detected in each population (Figure S6-7). The proportion of aneuploid samples in each population is shown on top of the bars.
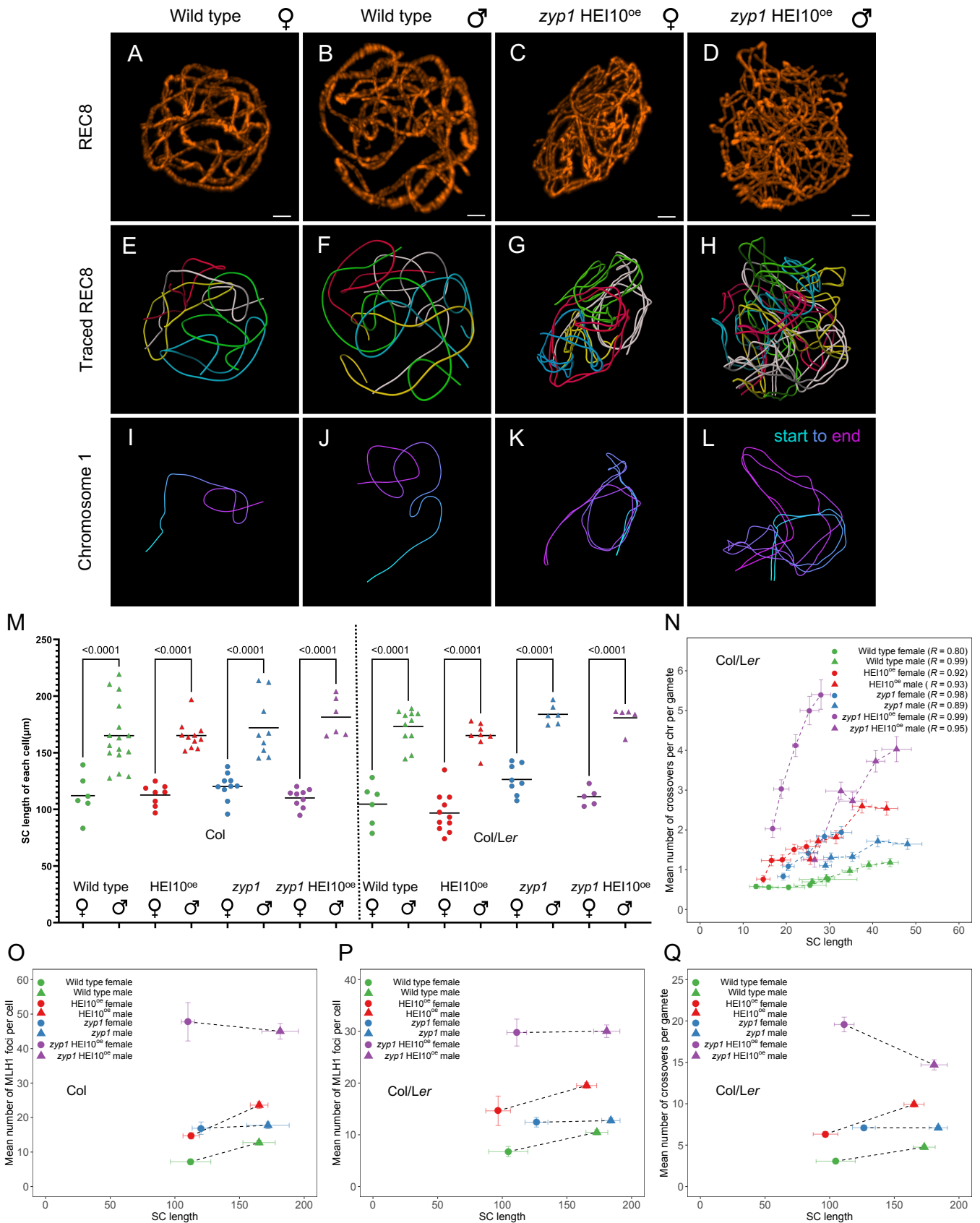
Figure 4. Analysis of SC/axis lengths in female and male meiocytes

(A–D) REC8 immunolocalization in female and male meiocytes of wild type and *zyp1* HEI10[oe homo] (Col). Imaging was done with 3D-STED and the projection is shown. Scale bar=1μm. (E–H) REC8 signal was traced in 3D. Each bivalent pair is color-coded. (I–L) Individual trace of the longest chromosome (presumably chromosome 1), with start-to-end color code. (M) Measurement of the total SC length. Each dot is the SC length of an individual cell. The bars indicate the mean. One-way ANOVA followed by Sidak correction showed that SCs were systematically longer in males than in females (p < 0.0001). The same test did not detect any differences between any of the pairs of males of different genotypes (p>0.4). For females, none of the pairwise comparisons were significantly different except in Col/L*er* HEI10[oe] that was lower than Col/L*er zyp1* (p=0.006) and Col *zyp1* (p=0.008). Note that variations in slide preparation and exact meiotic stage may affect this result. (N) Correlation analysis between the mean number of COs per chromosome per gamete and SC length (μm) in Col/L*er* background. SCs were attributed to specific chromosomes based on their length (e.g., the longest was presumably chromosome 1). Pearson's correlation coefficients are shown in parentheses. (O–P) The relationship between the mean number of MLH1 foci per cell and total SC length per cell in (O) Col background and (P) Col/L*er* background. (Q) The relationship between the mean number of COs per gamete and SC length in Col/L*er* background. The 90% confidence intervals are indicated as error bars.
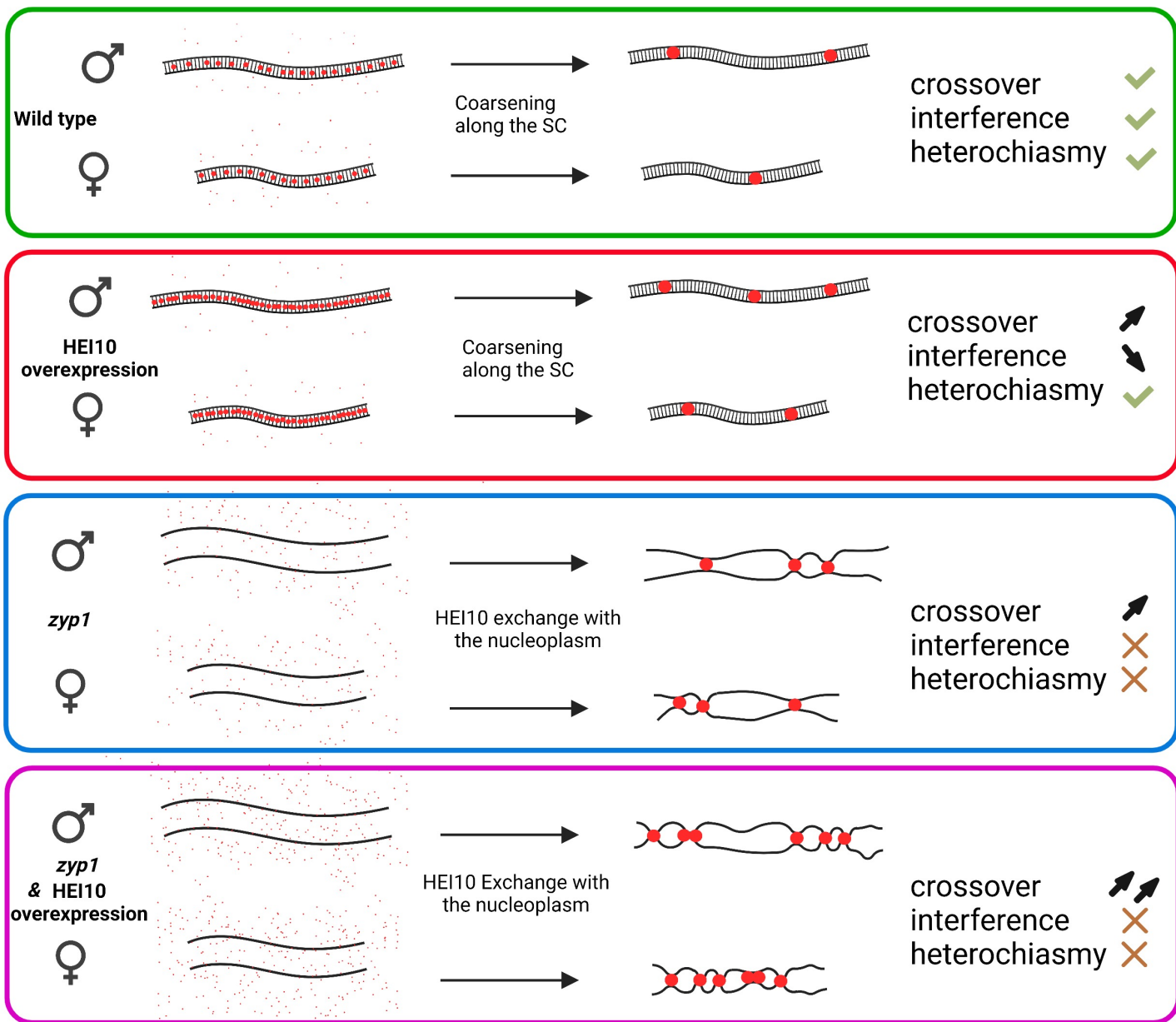
Figure 5. Model of crossover patterning *via* HEI10 coarsening

HEI10 (red) is captured by the central element of the SC and coarsens into large pro-CO droplets. The number of large pro-CO droplets is determined by SC length (heterochiasmy), and HEI10 expression levels. HEI10 overexpression increases CO number, and weakens interference but maintains heterochiasmy. In absence of an SC (*zyp1*), HEI10 is exchanged directly between the droplets and the nucleoplasm abolishing both interference and heterochiasmy, and the number of droplets depends on HEI10 expression level.
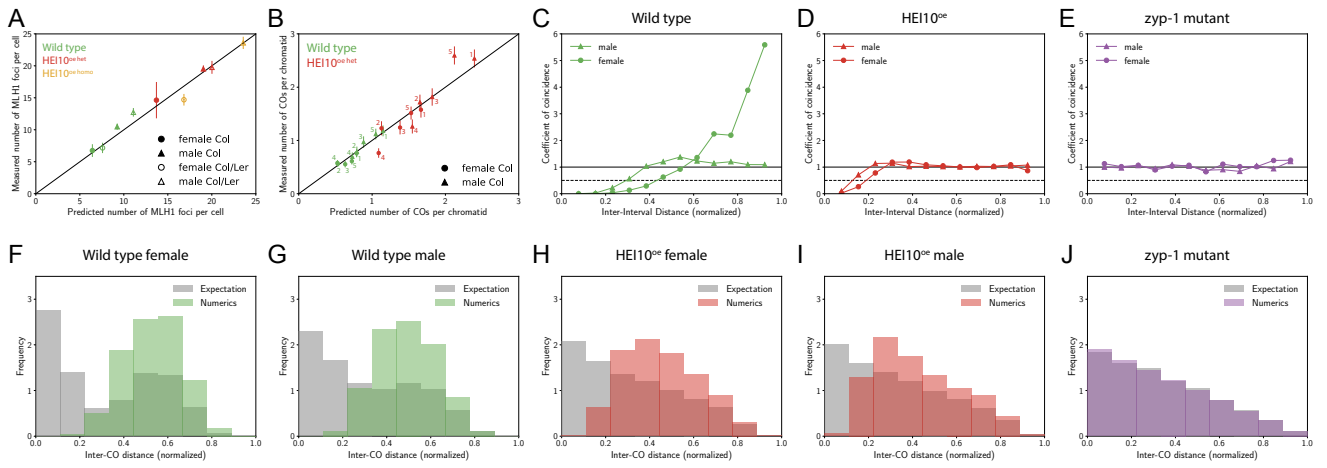
Figure 6. A coarsening model for crossover designation explains the measured data
(A) Number of MLH1 foci predicted by the model compared to the experimental measurements shown in Figure 1B. Error bars denote 90% confidence. (B) Number of COs per chromatid predicted by the model compared to the experimental measurements shown in Figure 1D. The respective chromatids are labeled and error bars denote 90% confidence. (C–E) Predicted coefficient of coincidence curves; compare to Figure 2G–J. (F–J) Predicted distributions of distances between two COs for chromosomes with exactly two COs; compare to Figure 2C–F. (A–J) Numerical details are given in the Methods. Mean and confidence intervals were determined from n=1000 (except n=500 in panel A) independent repetitions.